



**HAL**  
open science

## Development of a 3D and high resolution dynamic thermal model of a room with sun patch evolution for thermal comfort applications

Teddy Gresse, Lucie Merlier, Jean-Jacques Roux, Frédéric Kuznik

### ► To cite this version:

Teddy Gresse, Lucie Merlier, Jean-Jacques Roux, Frédéric Kuznik. Development of a 3D and high resolution dynamic thermal model of a room with sun patch evolution for thermal comfort applications. 2021 Building Simulation Conference, Sep 2021, Bruges, Belgium. 10.26868/25222708.2021.30827 . hal-04259427

**HAL Id: hal-04259427**

**<https://hal.science/hal-04259427>**

Submitted on 26 Oct 2023

**HAL** is a multi-disciplinary open access archive for the deposit and dissemination of scientific research documents, whether they are published or not. The documents may come from teaching and research institutions in France or abroad, or from public or private research centers.

L'archive ouverte pluridisciplinaire **HAL**, est destinée au dépôt et à la diffusion de documents scientifiques de niveau recherche, publiés ou non, émanant des établissements d'enseignement et de recherche français ou étrangers, des laboratoires publics ou privés.

## Development of a 3D and high resolution dynamic thermal model of a room with sun patch evolution for thermal comfort applications

Teddy Gresse<sup>1</sup>, Lucie Merlier<sup>2</sup>, Jean-Jacques Roux<sup>1</sup>, Frédéric Kuznik<sup>1</sup>

<sup>1</sup>Univ Lyon, INSA Lyon, CNRS, CETHIL, UMR5008, 69621 Villeurbanne, France

<sup>2</sup>Univ Lyon, UCBL, INSA Lyon, CNRS, CETHIL, UMR5008, 69622 Villeurbanne, France

### Abstract

The heterogeneous and transient features of indoor thermal environment play an important role in thermal comfort dynamics but remains difficult to predict accurately.

This contribution presents the development and validation of a detailed 3D building thermal model with high-resolution description of heat conduction in the envelope and surface balances. The model is applied to the evaluation of operative temperature distribution in a room with heterogeneous and transient radiative asymmetry.

It is intended to couple the model with computational fluid dynamics (CFD) in further works. The coupling would improve the numerical prediction of indoor thermal environments and could be used to study thermal comfort dynamics with high resolution boundary conditions.

### Key innovations

- Development of a detailed 3D building thermal model using C++ language and object-oriented programming.
- 3D mapping of the operative temperature over the whole room, showing the interest of such a model for heterogeneous and transient thermal environment with radiative asymmetry.
- Building model programming adapted for future coupling with CFD code.
- Intended application for thermal comfort analysis in transient and heterogeneous realistic indoor thermal environments.

### Practical implications

The model enables detailed calculation of wall and surface temperature fields with high spatial and temporal accuracy compared to classical building models. It may be used as a reference for benchmarks.

### Introduction

A building can be defined as a complex system where outdoor weather, building envelope, systems and occupants interact. The resulting thermal transfers are

mainly transient and heterogeneous. In addition, climate projections show an increase in strength and duration of heat waves during summer. With urban densification, concentrating people and strengthening urban heat island phenomena, the population exposed to urban overheating increases. Thus, buildings have to mitigate these effects while remaining energy conservative and ensure thermal comfort in particularly complex situations.

During periods of important heat stress, occupants may be immersed in various transient and heterogeneous indoor thermal environments such as asymmetric radiant fields, vertical temperature gradient, or localized and conditioned air flows. The dynamic response of human bodies to transient environments is correlated to the responses of the body's thermal receptors (Hensel (1981)). Under dynamic conditions, the thermoreceptors not only send a static signal based on skin and core temperature but also a dynamic signal based on the rate of change in both temperatures. The transient phase of the neural driven from a peripheral and core region is usually completed in less than 30s (Kenshalo et al. (1976)). In addition, Zhang (2003) shows that the overall comfort is mainly influenced by local sensation while the thermal sensation of the different body parts do not have the same impact on thermal comfort. Thus, thermal comfort involves multiple local and dynamic signals operating on diverse time scales, all superimposed on each other with different influential degree.

The most advanced development for numerical predictions of thermal comfort dynamics in transient and heterogeneous environments has been done in the area of multinode models of human thermal physiology and comfort. Recently, El Kadri (2020) proposed a new thermoregulation model of the human body based on neurophysiology called Neuro Human Thermal Model (NHTM) coupled with Zhang's thermal comfort model (Zhang (2003)). The model uses a time constant of 1.5s for the dynamic response of thermoreceptors. Thus, the strong spatial dependency and the fast temporal sensibility of thermal comfort dynamics suggest the need for a consistent modeling of indoor thermal environments. However, and to

our best knowledge, only building thermal models not adapted to the NHTM were applied to such human model so far.

Energy simulation programs generally aim to predict the energy consumption of buildings, like Energy Plus or Codyba. As a result, they consider thermal loads over a long period such as a year, and neglect or simplify some features of heat transfers. Conduction in the building envelope is typically considered 1D, short-wave radiation is projected on the floor and typical hourly weather data are used.

Hence, this contribution presents the development and the validation of a detailed dynamic thermal model designed to simulate a room for thermal comfort applications, using a 3D and high-resolution description of heat conduction in the envelope and surface balances. In particular, the model can handle short-time steps and calculates the sun patch, which corresponds to the projection of solar radiation through a window onto interior walls. The model is validated against experimental measurements carried out in the study of BESTLab full scale test cell (Rodler (2014)). The model is applied to calculate a 3D map of the operative temperature in the room for an heterogeneous and transient thermal environment with radiative asymmetry.

The next step will be to couple the building model with CFD to build a complete tool able to simulate realistic thermal environments with radiative and air-flow heterogeneous and transient features. Such simulations could be used as inputs of a thermophysiological human model for thermal comfort analysis.

## Model development

The model is developed using the C++ language, which is a powerful, efficient and fast language with many advantages. It allows to use object-oriented programming, a programming paradigm based on the concept of "objects", which can contain data in the form of attributes and code in the form of methods. This paradigm turns out to be well suited for building modeling and facilitates the model maintenance. It prevents to manipulate large matrices and calculate, for example, matrix inversion. Moreover, C++ has a rich and optimized function library useful for mathematic calculations in the model.

The object-oriented programming of the model allows the definition of five main objects:

- *Cells*: The walls of the room are modeled as a finite element mesh made up of 3D elements.
- *Surfaces*: A wall is composed of two surfaces: an internal and an external one.
- *Facets*: A surface is subdivided in smaller 2D elements called facets that represent the direct interface between the boundary cells and the environment (external or internal).
- *Room*: The room is represented, in a first ap-

proach, as a single node with a unique temperature.

- *Window*: To account for the solar gains in the room, a window can be added in the model.

Each object has specific attributes and methods and interact with the others at every time step to calculate accurately the 3D thermal behaviour of a room.

### Cell

Within a wall, heat transfer is only governed by conduction. The thermal behaviour of the cell  $(i, j, k)$  is governed by the 3D heat equation resolved using an explicit Euler scheme:

$$\rho_{i,j,k} C_{i,j,k} V_{i,j,k} \frac{\Delta t (T_{i,j,k})}{\Delta t} = K_{i-1/2,j,k} (T_{i-1,j,k} - T_{i,j,k}) + K_{i+1/2,j,k} (T_{i+1,j,k} - T_{i,j,k}) + K_{i,j-1/2,k} (T_{i,j-1,k} - T_{i,j,k}) + K_{i,j+1/2,k} (T_{i,j+1,k} - T_{i,j,k}) + K_{i,j,k-1/2} (T_{i,j,k-1} - T_{i,j,k}) + K_{i,j,k+1/2} (T_{i,j,k+1} - T_{i,j,k}) \quad (1)$$

where  $\rho$  ( $kg/m^3$ ) is the wall material density,  $C$  ( $J/(Kg.K)$ ) is the wall material heat capacity,  $V$  ( $m^3$ ) is the cell volume,  $K$  ( $W/K$ ) are the conductances at the interface between the cell and the adjacent ones,  $T_{i,j,k}$  ( $K$ ) is the cell temperature, and the other temperatures belong to the six adjacent cells. These variables constitute the cell's attributes in the model. The conductance  $K_{i+1/2,j,k}$  between the cell  $(i, j, k)$  and the cell  $(i + 1, j, k)$ , for exemple, is calculated as follows:

$$K_{i+1/2,j,k} = \frac{\delta y_j \delta z_k}{\delta x_i / 2 \lambda_{i,j,k} + \delta x_{i+1} / 2 \lambda_{i+1,j,k} + R_{i+1/2,j,k}} \quad (2)$$

where  $\lambda_{i,j,k}$  and  $\lambda_{i+1,j,k}$  ( $W/(m.K)$ ) are the thermal conductivities of the cell  $(i, j, k)$  and  $(i + 1, j, k)$  respectively,  $R_{i+1/2,j,k}$  ( $m^2.K/W$ ) is thermal resistivity of the interface between these two cells and  $\delta x_i$ ,  $\delta y_j$  et  $\delta z_k$  ( $m$ ) refer to the cell dimensions in the 3 space directions.

### Surface

The wall surfaces have specific optical properties like emissivity, reflectivity and absorbtivity. Moreover different boundary conditions can be applied over the surfaces: temperature or flux conditions, which can be fixed or floating.

### Facet

When convective and radiative fluxes (shortwave (SW) and longwave (LW) contributions) are considered as boundary condition on the associated surface of the boundary cells  $(1, j, k)$  for example, a heat balance is calculated over the facet:

$$\phi_{facet,1,j,k}^{cond} + \phi_{facet,1,j,k}^{conv} + \phi_{facet,1,j,k}^{rad,SW} + \phi_{facet,1,j,k}^{rad,LW} = 0 \quad (3)$$

This equation is solved by the TOMS 748 algorithm (Alefeld et al. (1995)), a root-finding without derivatives method from the C++ Boost library.

*Conductive heat transfer:*

The heat flow  $\phi^{cond}$  ( $W/m^2$ ) from the boundary cell  $(1, j, k)$  to its boundary facet is given by equation (4):

$$\phi_{facet,1,j,k}^{cond} = K_{1/2,j,k} (T_{1,j,k} - T_{facet,1,j,k}) \quad (4)$$

where  $K_{1/2,j,k}$  is the conductance between the boundary cell  $(1, j, k)$  and its boundary facet and  $T_{1,j,k}$  and  $T_{facet,1,j,k}$  are the temperatures of the boundary cell  $(1, j, k)$  and the boundary facet respectively.

*Convective heat transfer:*

Equation (5) gives the convective heat flux  $\phi^{conv}$  ( $W/m^2$ ) between the indoor or outdoor environment and the wall boundary facet:

$$\phi_{facet,1,j,k}^{conv} = h_{facet,1,j,k} S_{facet,1,j,k} (T_a - T_{facet,1,j,k}) \quad (5)$$

where  $h_{facet,1,j,k}$  is the convective heat transfer coefficient (CHTC),  $S_{facet,1,j,k}$  ( $m^2$ ) is the facet area and  $T_a$  ( $K$ ) the indoor or outdoor air temperature. The CHTC is calculated with empirical correlations: the correlation from McAdams (1954) for outdoors and the correlation from Awbi and Hatton (1999) for indoors.

*Radiative heat transfer:*

The radiative flows  $\phi^{rad,LW}$  and  $\phi^{rad,SW}$  ( $W/m^2$ ) are calculated with the progressive refinement radiosity algorithm (Cohen et al. (1988)), based on the concept of shooting flux depicted in figure 1. The methodology is adapted from Ashdown (2002).

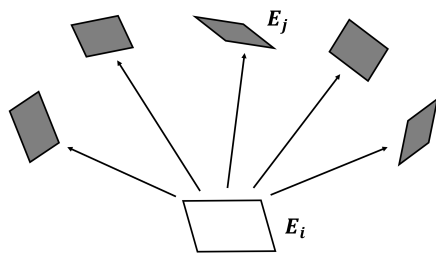


Figure 1: Shooting flux concept.

This approach corresponds to shoot flux from one facet  $E_i$  to the others  $E_j$ . These facets then become secondary sources, shooting some of the flux they receive back into the environment, by always selecting the element that has the greatest amount of flux to “shoot”. This process continues until the total amount of flux remaining in the environment is less than a predetermined fraction. Equation (6) gives the shooting flux (exitance  $M_{ji}$ ) of the receiving facet  $E_j$ :

$$M_{ji} = \rho_j M_i F_{ji} \quad (6)$$

with  $\rho_j$  the reflectance of the facet  $E_j$  and  $F_{ij}$  the form factor from the facet  $E_j$  to the facet  $E_i$  computed using the hemicube methods.

This leads to a radiative balance over the interior facets which take into account the multi-reflexions. Thus, the net flux density  $\phi_i$  ( $W/m^2$ ) over the facet  $E_i$  is calculated as:

$$\phi_i = I_{r0,i} + \alpha_i \sum_j M_j \cdot F_{ij} - M_{0,i} \quad (7)$$

where  $I_{r0,i}$  and  $M_{0,i}$  ( $W/m^2$ ) are the initial irradiance and exitance of the facet respectively,  $\alpha_i$  is the SW absorptivity of the facet and  $M_j$  ( $W/m^2$ ) is the exitance of the other facets  $E_j$ .

For the long wave contribution, the initial facet exitance is calculated by the Stephan-Boltzmann law.

On one hand, for the short wave contribution, the transmitted diffuse solar radiation is considered as the initial exitance of the window interior facets. On the other hand, the transmitted direct solar radiation, i.e. the sun patch, is determined by a geometrical test on the projection of the center of the interior facets and the window frame onto the plan  $N$  perpendicular to the sun rays as depicted on figure 2. Note that no other building is considered outside to prevent potential shading effects and facilitate the detection. The initial exitance corresponds to the reflected fraction, considered as fully diffuse, of the direct solar radiation transmitted by the window and received by the facets detected into the sun patch. The initial irradiance, for its part, corresponds to the absorbed fraction of the solar radiation.

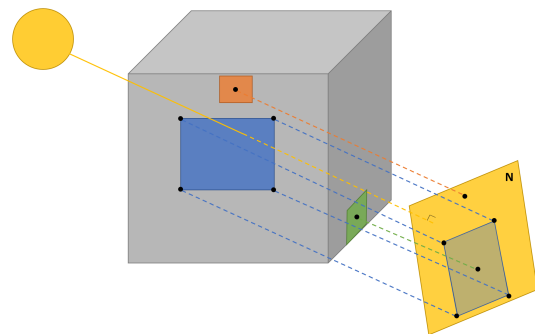


Figure 2: Projection of the window frame and the center of interior facets onto the plan  $N$  perpendicular to the sun rays.

**Room**

The indoor environment is modeled as a single air node for the air temperature calculation. An energy balance in the room with air temperature  $T_{ai}$  ( $K$ ) is calculated using an explicit Euler scheme:

$$\rho_{air} C_{air} V_r \frac{\Delta_t T_{ai}}{\Delta t} = \sum_{n=0}^N \dot{m}_n \cdot C_{air} (T_{ae} - T_{ai}) + \sum_{n=0}^{NM} S \cdot h_{ci} (T_{SI} - T_{ai}) \quad (8)$$

where  $\rho_{air}$  ( $kg/m^3$ ) is the the air density,  $C_{air}$  ( $J/kg.K$ ) is the heat capacity of the air,  $V_r$  ( $m^3$ )

is the volume of the room,  $N$  is the number of external zones,  $\dot{m}$  ( $kg/s$ ) is the leakage rate with the corresponding zone,  $T_{ae}$  ( $K$ ) is the dry bulb temperature of the corresponding zone,  $NM$  is the number of surface facets,  $S$  ( $m^2$ ) is the area of the surface mesh element,  $h_{ci}$  is the CHTC,  $T_{SI}$  ( $K$ ) is the interior surface temperature. The air properties, the leakage rate and the geometric characteristics define the attribute of this objects.

### Inputs of the model

The input data are the building characteristics (location, wall composition, surface radiative properties, room air properties), the specific temperatures for fixed boundary conditions and the meteorological measurements.

The numerical mesh of the room is generated with HEAT3 in cartesian coordinates (Blomberg (1996)).

## Case study

### Experimental test cell

A full scale low-energy test cell called BESTLab developed in EDF R&D laboratory (latitude :  $48^{\circ}22'$  N; longitude :  $2^{\circ}49'$  E; altitude : 100m) and experimentally studied by Rodler (2014) is chosen for the model validation.

The cubic room dimensions are 2.97 m in width 2.90 m in depth and 2.82 m in height. The room West facing outside wall is equipped with a double glazing window and the three other vertical walls are surrounded by a thermal guard. An isolated closed door on the East wall gives access to the thermal guard. The room is represented figure 3.

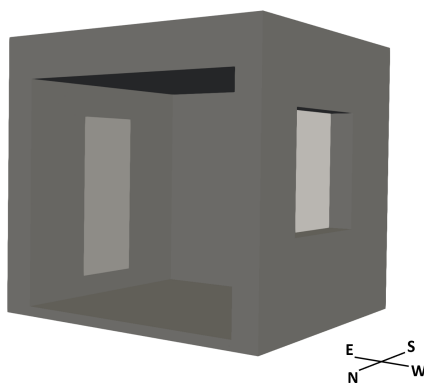


Figure 3: BESTLab test cell geometry with a door on the East wall and a window on the West wall. The North wall is removed to see inside the room.

The walls are made of different materials such as coat, plaster or insulation disposed in consecutive layers. As a result, the East, South and North walls are 41 cm thick and the West wall is 32.4 cm thick. The thermal characteristics of the materials as well as the characteristics of the window are given in Rodler (2014).

Ten PT100 probes, numbered 1 to 10, were installed at different locations on the interior wall surfaces to measure the wall surface temperature as represented

in figure 4. The indoor air temperature was measured with three radiation shielded PT100 probes, respectively called probe A1, A2 and A3, located at the bottom, the middle and the top of the room volume to take into account a potential heterogeneity of temperature due to stratification.

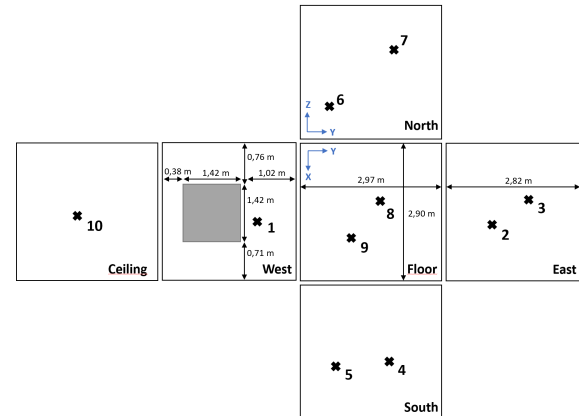


Figure 4: Surface probes positioning on the internal wall surfaces.

### Model settings

The test cell geometry and the composition of the walls are accurately modeled with HEAT3 thanks to a 3D mesher and a building materials library available in the software.

The exterior boundary conditions are either fluxes or temperatures. The West facing wall is in contact with the outside air and receive solar radiation. The three other walls are surrounded by a thermal guard with a constant air temperature of  $20^{\circ}C$ . Thus, only the convective flux is considered on these walls. A constant temperature of  $19^{\circ}C$  is applied on the floor and the roof external surfaces, as measured in the experimental study.

Minute-wise weather data were used from the meteorological station "Les Renardières" of EDF Lab site. The outdoor temperature, humidity, sun radiation and wind conditions were taken from the measurements performed in the direct vicinity of BESTLab test cell. No other building surround the test cell.

The period used for the validation is a week from the 8th of May to the 16th of May 2013.

Previous numerical studies were carried out by Rodler (2014) to assess the importance of the weather data sampling and to analyze and optimize the mesh size for this room, which gave the discretization presented in figure 5. The resulting mesh is composed with 22780 cells, 5300 exterior facets and 560 interior facets.

## Validation

Three days of initialization were simulated to remove the initial conditions influence while accounting for the real environmental history.

Our simulation has a time step of 4.08s. It took about

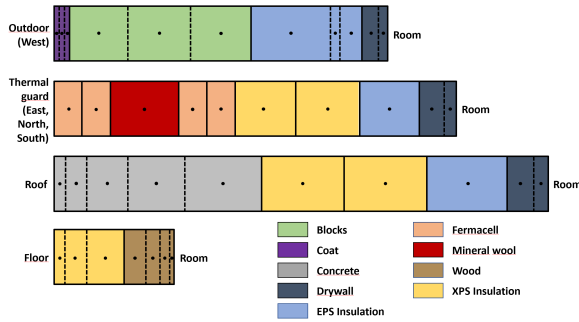


Figure 5: Wall materials and discretization in the test cell BESTLab.

24h over one processor (Intel(R) Xeon(R) CPU E5-2670 v2 @ 2.50GHz) to run the 8 days of simulation. Results are minute-averaged to be compared with experiment.

To validate the model, two indicators were selected to evaluate statistically the discrepancies between measurements and simulations:

- the Root Mean Square Error (RMSE) in °C:

$$RMSE = \sqrt{\frac{\sum_{i=1}^{N_T} (T_{meas}(i) - T_{sim}(i))^2}{N_T}} \quad (9)$$

where  $T_{meas}$  and  $T_{sim}$  (K) are the measured and simulated temperatures and  $N_T$  is the number of data samples.

This indicator measures the accuracy of the simulated temperatures against the measured temperatures. A value close to zero, or at least less than one, traduces an overall good correlation.

- the Error in Daily Maximum ( $\Delta T|_{max}$ ) in °C:

$$\Delta T|_{max} = (T_{max,sim} - T_{max,meas})|_{day} \quad (10)$$

where  $T_{max,meas}$  and  $T_{max,sim}$  (K) are the maximal measured and simulated temperatures over a day of the study period.

This indicator is useful to evaluate the consistence of the temperature peaks induced by abrupt changes in thermal loads.

## Results

**Room surface temperatures** Figures 6, 7, 8 and 9 compare the measured and simulated surface temperatures at probes 2, 4, 7 and 8 respectively. Probes 2, 4 and 8 receive direct and diffuse sun radiation. Probe 7 receive only diffuse radiation. The other probes also receive only diffuse solar radiation. The surface temperature evolution over these probes are similar leading to the same observations as for probe 7. Table 1 gives the corresponding Error in Daily Maximum and RMSE indicators.

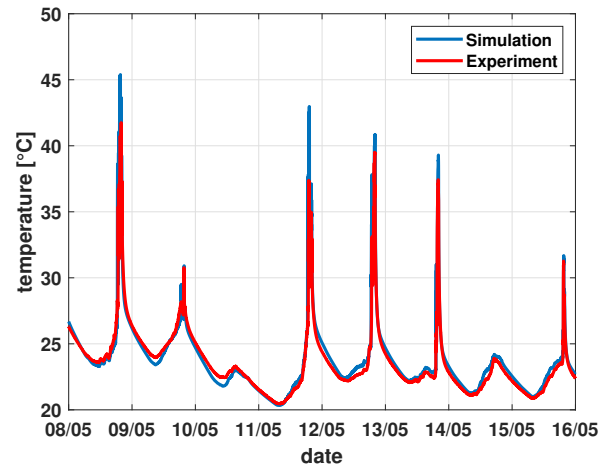


Figure 6: Measured and simulated surface temperature at probe 2 (on the East wall).

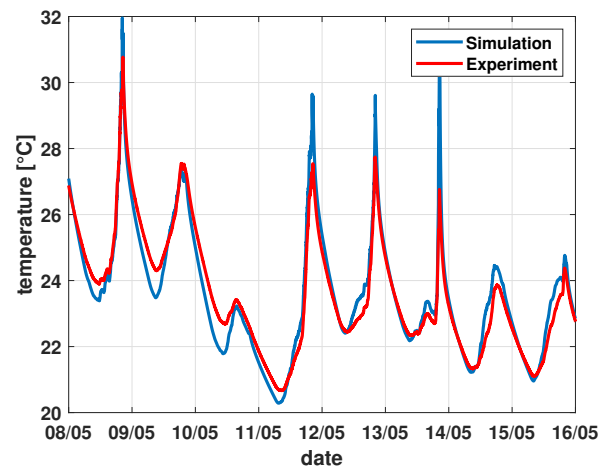


Figure 7: Measured and simulated surface temperature at probe 4 (on the South wall).

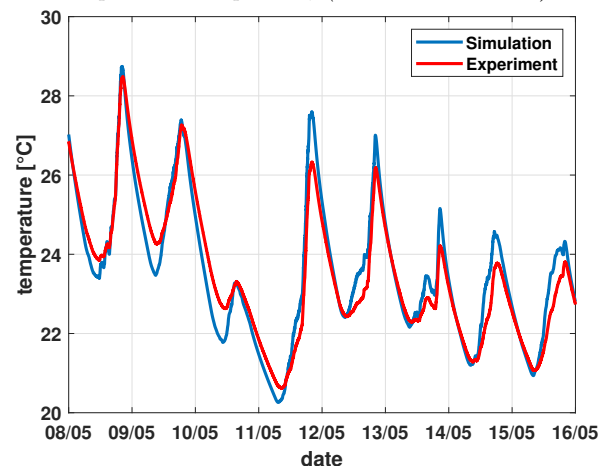


Figure 8: Measured and simulated surface temperature at probe 7 (on the North wall).

Table 1: Error in Daily Maximum and RMSE between measurements and simulations for surface temperature at the corresponding probes.

Probe Wall	2 East	4 South	7 North	8 Floor
$\Delta T _{max}$ (°C)	5.59	3.94	1.26	3.90
RMSE (°C)	0.90	0.52	0.51	0.60

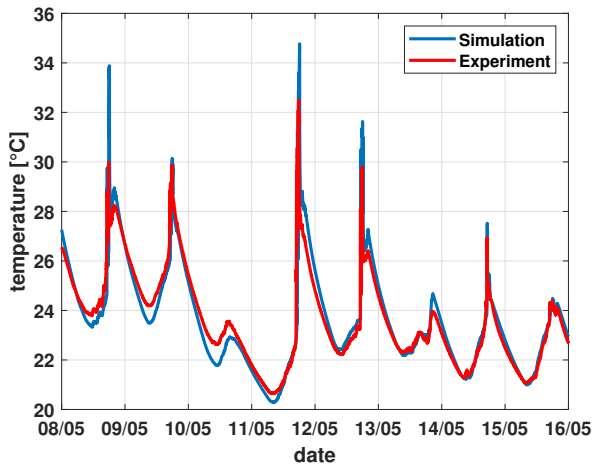


Figure 9: Measured and simulated surface temperature at probe 8 (on the floor).

**Room air temperature** The room air temperature measured by probe A2 is chosen for the comparison with the simulated one.

Figure 10 compare the measured and simulated room air temperatures. Table 2 gives the corresponding Error in Daily Maximum and RMSE indicators.

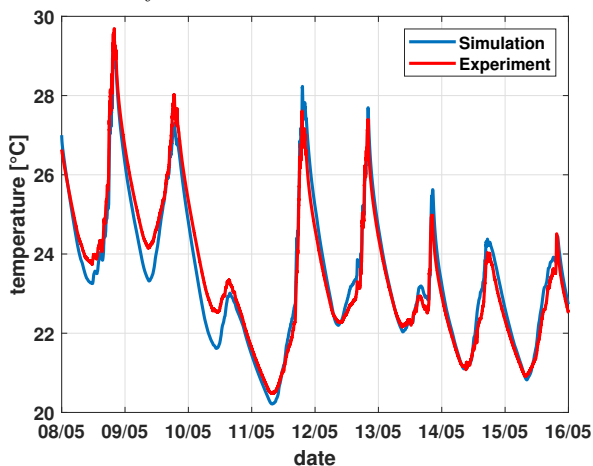


Figure 10: Measured and simulated room air temperature.

Table 2: Error in Daily Maximum and RMSE between measurements and simulations for room air temperature.

Probe	Air
$\Delta T _{max}$ (°C)	0.74
RMSE (°C)	0.42

### Analysis

The overall trend of the simulated temperatures are in good agreement with measurements. During days with important direct solar radiation, the model predicts well the temperature peaks in terms of time occurrence. On more cloudy days, such as the 10th of May and the 14th of May, the simulated temperatures are consistent with the measurements traducing a correct diffuse radiation distribution on the room.

Still, there are noticeable differences such as an underprediction of night surface and air temperatures

the first three days of the analyzed period and an overprediction of the temperature peaks intensity induced by the sun patch. These differences can be attributed to the combined effects of error propagation in inputs and outputs:

- Inputs: on-site weather data measurement error, use of standard material properties that may not fully represent building materials, errors due to modeling approximation (especially simplification in geometry).
- Outputs: nodal representation of the room air volume, use of empirical CHTC correlations, sensor measurement errors due to the acquisition chain.

Tables 1 and 2 show the values of the error analysis indicators for the studied period. The results highlight:

- Probes which detect sun patch during sunny days have higher RMSE and  $\Delta T|_{max}$  values. The higher the surface temperature, the larger the discrepancy.
- $\Delta T|_{max}$  values vary from about 1°C to almost 6°C at probes receiving sun patch. However, no conclusion can be drawn with this indicator because of the lack of propagation error in the experimental acquisition chain that can be significant with high solar gains.
- RMSE values are all below 1 which confirms the good agreement between measurements and simulations.

### Application

A first approach for thermal comfort evaluation is the calculation of the operative temperature in the room. In homogeneous thermal environments, the operative temperature is based on mean radiant temperature and air temperature. If the radiative environment has a strong radiative heterogeneity, like in the case studied, the radiative asymmetry must be considered in the operative temperature calculation.

The operative temperature calculation is based on a heat balance over a virtual black globe taking into account the convective heat transfer, the radiant temperature and the SW radiative heat flux:

$$S\epsilon\sigma(T_{op}^4 - T_{rad}^4) + Sh_{conv}(T_{op} - T_{air}) + \alpha I_{g,\tau} S_{app} = 0 \quad (11)$$

where  $I_{g,\tau}$  ( $W/m^2$ ) is the solar heat flux transmitted by the window and received by the black globe,  $S$  ( $m^2$ ) is the surface of the globe,  $S_{app}$  ( $m^2$ ) is the apparent surface of the globe,  $\alpha$  and  $\epsilon$  are the associated SW absorptivity and LW emissivity.

The CHTC correlation from Inard (1988) is used:

$$h_{conv} = \left(1.14 + \frac{0.17}{D_{gb}}\right) (T_{op} - T_{air})^{0.25} \quad (12)$$

where  $D_{gb}$  is the diameter of the globe.

The radiant temperature ( $K$ ) is calculated using (13) considering the LW heat transfer between the black globe and the wall facets:

$$T_{rad} = \sqrt[4]{\sum_{j=1}^{N_f} F_{O,j} T_{f,j}^4} \quad (13)$$

where  $F_{O,j}$  is the form factor between the globe and the wall facet  $j$ ,  $T_{f,j}$  ( $K$ ) is the temperature of the facet  $j$  and  $N_f$  is the number of interior wall facets.

For a black globe located in the middle of the room, the air temperature and operative temperature simulated the 8th of May 2013, the day with the maximum air temperature over the studied week, are depicted figure 11. It shows a strong deviation of about  $10^{\circ}\text{C}$  between the air temperature and the operative temperature by the end of the day when the sun patch hits the black globe. This important increase of the operative temperature may cause thermal discomfort.

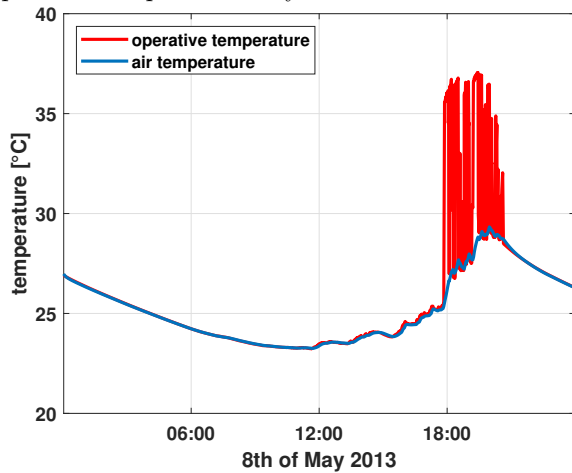


Figure 11: Air temperature and operative temperature in the middle of the room.

The maximum operative temperature during the same day is recorded at 5:24 PM. At this moment, the East wall of the room is heated locally, up to  $46^{\circ}\text{C}$ , by an important SW heat flux leading to a significant surface temperature heterogeneity as shown by figure 12. This non-uniform surface temperature and the SW heat flux distributions suggest a spatial heterogeneity of the operative temperature in the room.

A 3D mapping of the operative temperature is operated in the whole room. It requires the discretization of the indoor room air volume to model the radiative heat flux distribution. Figures 13 and 14 depict the spatial distribution over an horizontal plane P1 and a vertical plane P2 respectively. It shows a variation from  $29^{\circ}\text{C}$  outside of the solar beam to more than  $40^{\circ}\text{C}$  close to the East wall in the sun patch. This traduces the importance of the SW heat flux in the heat balance for operative temperature calculation within the solar beam. Moreover, the LW heat flux from the

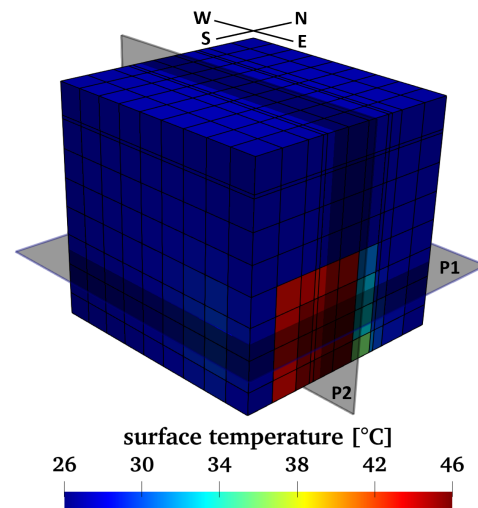


Figure 12: Interior surface temperature (3D exterior viewpoint) the 8th of May 2013 at 5:24 PM with two horizontal and vertical planes P1 and P2.

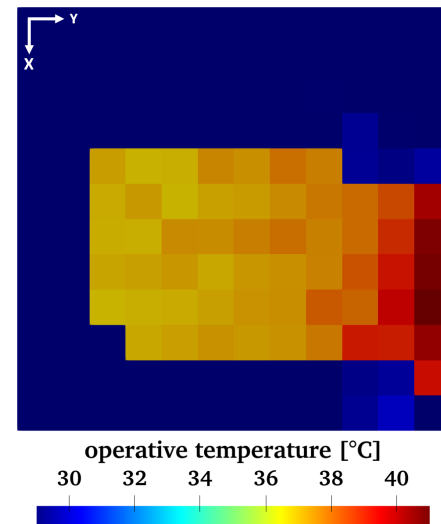


Figure 13: Operative temperature field in the room over the plane P1 the 8th of May 2013 at 5:24 PM.

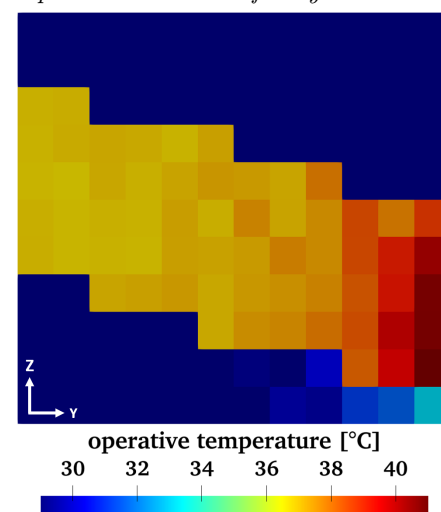


Figure 14: Operative temperature field in the room over the plane P2 the 8th of May 2013 at 5:24 PM.

heated wall facets has a significant impact as well: a temperature gradient is noteworthy within the solar

beam, with operative temperature varying from 37°C far from the heated surface to 41°C closer. The heterogeneity of the operative temperature distribution in the room can induce local thermal discomfort.

The spatial and temporal dependency of the operative temperature highlights the need for a detailed and accurate 3D building model to predict thermal comfort in heterogeneous and transient radiative environments. Such thermal environments with radiative asymmetry are intensified during urban overheating period in summer and are, therefore, of main concern. Thus, the model, with its spatial and temporal characteristics, has proven to be a promising tool for thermal comfort analysis in complex thermal environments.

### Conclusion and perspectives

Usual energy simulation programs generally aim to predict the energy consumption of buildings over a year and are not suited to the study of thermal comfort dynamics, which was shown to be strongly dependent on the spatial distribution of environmental variables and sensitive to rapid dynamics.

Thus, the development of a 3D thermal model with high spatial and temporal resolution using object oriented paradigm with C++ language was introduced. The detailed modeling of radiative contributions allow the sun patch detection and the inclusion of radiative multireflexions. The validation of the model with the experimental measurements carried out on the low-energy test cell BESTLab from Rodler (2014) shows an overall good agreement in room surface temperature and room air temperature prediction. The selected indicators statistically confirmed the validity of the model but bring to light some discrepancies that partly reflect weaknesses in the indoor air volume modeling and the associated convective heat transfers approach. The model was then applied to analyze the operative temperature distribution in thermal environment with strong radiative asymmetry due to sun patch. Results show a significant operative temperature heterogeneity and temporal dependency leading to a potential thermal discomfort. This confirms the necessity of such a detailed building model to accurately predict heterogeneous and transient thermal environments. An extended study about the operative temperature dynamics, when sun patch disappear for example, could reveal interesting features about the rapid temporal evolution of the operative temperature distribution.

The next step will be to couple this building thermal model with CFD based on Large Eddy Simulation approach (LES) to capture the dynamic structures of indoor airflows that may have significant impacts on thermal comfort dynamics. The final objective will be to assess thermal comfort in a realistic heterogeneous and transient indoor thermal environments by adding

a numerical thermal manikin to the coupling such as the NHTM from El Kadri (2020).

### Acknowledgment

I would like to thank Auline Rodler for providing us with the data of the test cell BESTLab and for her useful advice. I also thank EDF as part of "buildings with high energy efficiency" (BHEE) joint laboratory which funded the experimental research carry out on BESTlab test cell.

### References

- Alefeld, G. E., F. A. Potra, and Y. Shi (1995). Algorithm 748: enclosing zeros of continuous functions. *ACM Transactions on Mathematical Software*.
- Ashdown, I. (2002). *Radiosity: A Programmer's Perspective*. Wiley.
- Awbi, H. B. and A. Hatton (1999). Natural convection from heated room surfaces. *Energy and Buildings*.
- Blomberg, T. (1996). *Heat conduction in two and three dimensions: computer modelling of building physics applications*. Ph. D. thesis, Lund University.
- Cohen, M. F., S. E. Chen, J. R. Wallace, and D. P. Greenberg (1988). A progressive refinement approach to fast radiosity image generation. *SIGGRAPH Comput. Graph.*
- El Kadri, M. (2020). *Modèle thermoneurophysiologique du corps humain pour l'étude du confort thermique en conditions climatiques hétérogènes et instationnaires*. Ph. D. thesis, Université de la Rochelle.
- Hensel, H. (1981). Thermoreception and temperature regulation. *Monographs of the Physiological Society*.
- Inard, C. (1988). *Contribution à l'étude du couplage thermique entre un émetteur de chaleur et un local*. Ph. D. thesis, INSA, Lyon.
- Kenshalo, D. R., D. Cormier, and M. Mellos (1976). Some response properties of cold fibers to cooling. *Progress in Brain Research*.
- McAdams, W. H. (1954). *Heat Transmission*. McGraw-Hill Kogakusha.
- Rodler, A. (2014). *Modélisation dynamique tridimensionnelle avec tache solaire pour la simulation du comportement thermique d'un bâtiment basse consommation*. Ph. D. thesis, INSA, Lyon.
- Zhang, H. (2003). *Human Thermal Sensation and Comfort in Transient and Non-Uniform Thermal Environments*. Ph. D. thesis, University of California, Berkeley.